ASYMMETRIC MAGNETIC ANOMALIES OVER TWO YOUNG IMPACT CRATERS ON MERCURY

Valentina Galluzzi[1], **Joana S. Oliveira**[2,3], Jack Wright[4], Lon L. Hood[5], David A. Rothery[4]

[1] INAF, Istituto di Astrofisica e Planetologia Spaziali, Rome, Italy
[2] ESA/ESTEC, SCI-S, Noordwijk, Netherlands
[3] CITEUC, Geophysical and Astronomical Observatory, University of Coimbra, Coimbra, Portugal
[4] School of Physical Sciences, The Open University, Milton Keynes, UK
[5] Lunar and Planetary Laboratory, University of Arizona, Tucson AZ, USA

EGU General Assembly 2020

INTRO

The crustal magnetic field of the northern hemisphere of Mercury includes some magnetic anomalies, far from the Caloris basin that are correlated with other impact craters [Hood et al., 2018]. Although Mercury's surface has a low iron abundance, it seems likely that some impactors brought magnetic carriers that could register the magnetic field of Mercury after impact. Anomalies associated with Rustaveli and Stieglitz craters [Fig. 1] are slightly or totally asymmetric with respect to the crater center. We analyze the shape of the anomalies and the impact crater morphologies to understand whether there is any connection between the impactor and the anomalies. The morphology and geological setting of these two fresh impact craters that still maintain a well-preserved ejecta blanket and visible secondary crater chains are investigated to constrain the overall impact dynamics.

In the last months of its mission, MESSENGER was able to obtain measurements at low altitude (< 120 km). This has made it possible to measure small magnetic field signals, probably of crustal origin [Johnson et al, 2015].

Maps of the crust signatures at 40 km altitude were produced by Hood [2016] and Hood et al. 2018 [Fig. 1], showing that the strongest anomalies are about 9.5 nT in the Caloris basin.
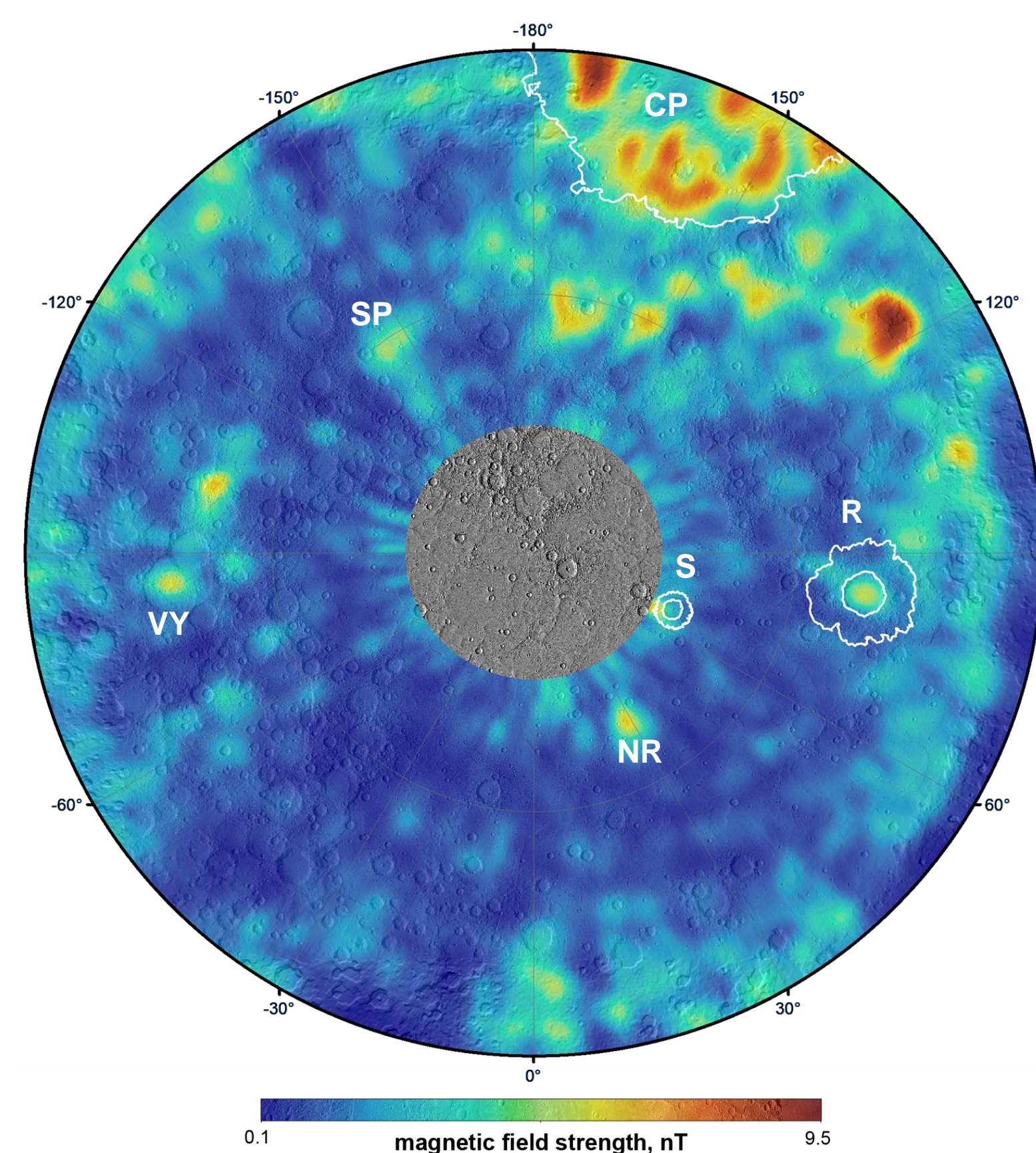
Figure 1 | Magnetic field intensity at 20 km altitude superposed on a Mercury Laser Altimeter (MLA) shaded relief basemap in stereographic north pole projection (from 35°N to 90°N). Caloris Planitia and Rustaveli and Stieglitz craters with their ejecta are shown with white contours.

R = Rustaveli;
S = Stieglitz;
V = Vyasa;
NR = Northern Rise;
SP = Suisei Planitia;
CP = Caloris Planitia

Some of the anomalies are associated with impact craters, and it has been demonstrated that this is not a coincidence [Hood et al. 2018]. It is believed that these anomalies are the result of impactors material rich in magnetic carriers that were incorporated on the surface acquiring remanent magnetic fields during the cooling of the material.

The incorporation of the impactor material depends on several variables: velocity, angle and composition of the impactor and composition of the surface area [Wieczorek et al., 2012].

AIM

We intend to analyze whether the anomalies of the crustal field are related to geological characteristics by means of 1) geomorphological analysis, 2) crater chain distribution analysis, and 3) impact dynamics evaluation in order to test this impactor hypothesis.

STIEGLITZ CRATER | 67.63°E; 72.53°N

Stieglitz crater is a **mature complex crater** ~95 km in diameter located on the eastern limit of the Northern Rise and superposed on the smooth plains of Borealis Planitia. Based on overlapping crater densities and morphological appearance it is the youngest crater of its size in its surrounding area [Fig. 2a].
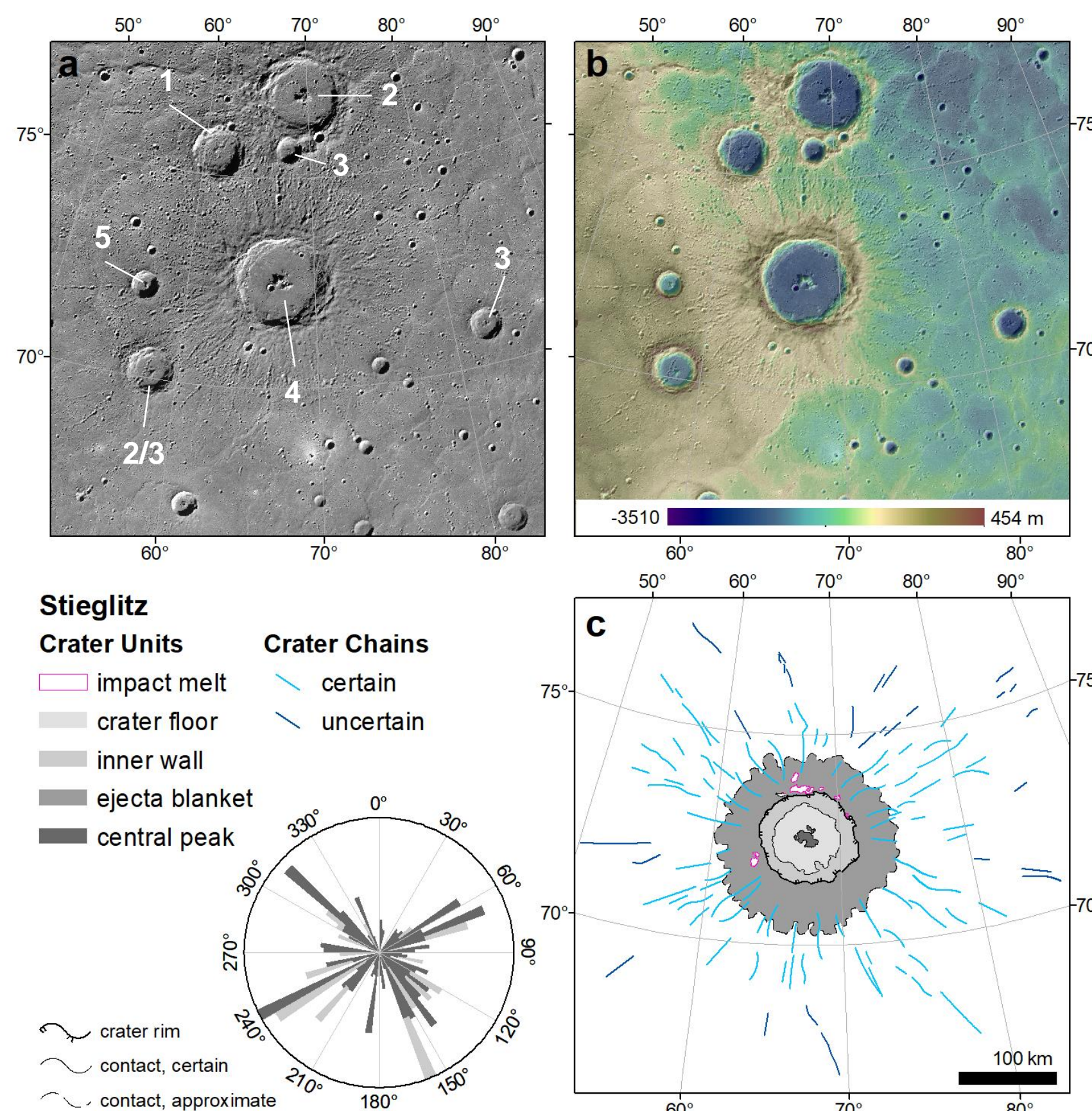

Figure 2 | Stieglitz crater in stereographic projection centered on the crater center (67.63°E; 72.53°N): **a)** Relative age of Stieglitz and the surrounding craters from the oldest (1) to the youngest (5) on the HIE (High-Incidence from East) basemap at 166 m/pixel; **b)** MLA DTM; **c)** Simplified geological map showing the trend of certain and uncertain secondary crater chains related to the Stieglitz impact. **Bottom-left:** rose diagram analysis of crater chains showing the start and end azimuth of chains indicated by the dark and light bins, respectively.

A | The rim is slightly higher in the arc centered at SW than on the opposite side; the deepest chain is located to the N of the crater [Fig. 2b].

B | Symmetrical continuous ejecta blanket that extends up to ~one crater radius from the rim crest, but slightly further in the SW. There is a slight lack of crater chains NNE of the crater [Fig. 2c].

**C |** The U-shaped central peak opens towards SW.

D | Melt pools are clustered on the northern part of the blanket, minor pools are found SW.
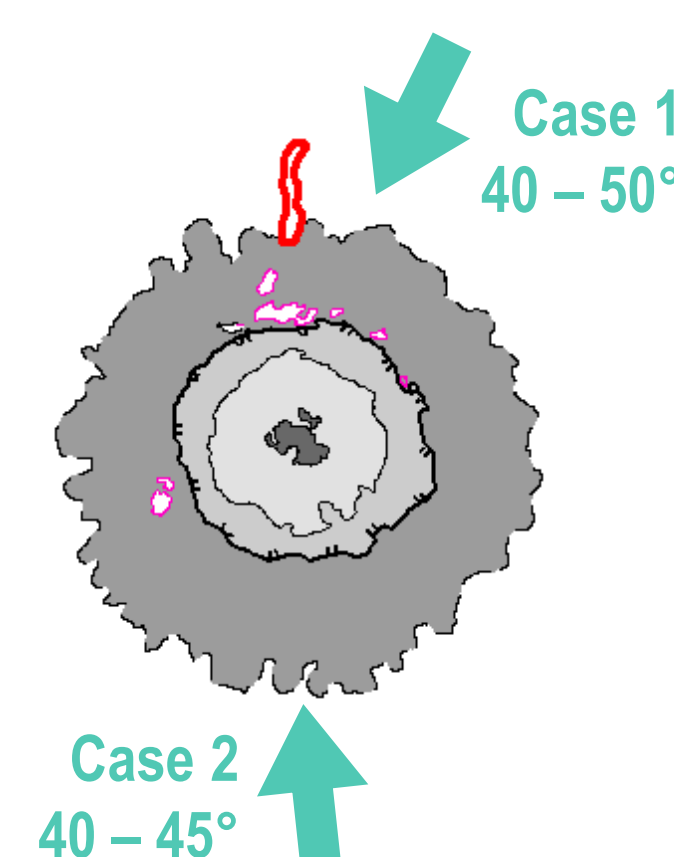
RUSTAVELI CRATER | 82.74°E; 52.41°N

Rustaveli crater is a **peak-ring basin** ~210 km in diameter located in the northeast of Mercury's Hokusai quadrangle [Wright et al., 2019]. As Stieglitz, it superposes the smooth plains of Borealis Planitia. A secondary infilling of smooth plains obscures the original floor and only the tops of the basin's peak-ring elements are visible [Fig. 4a].
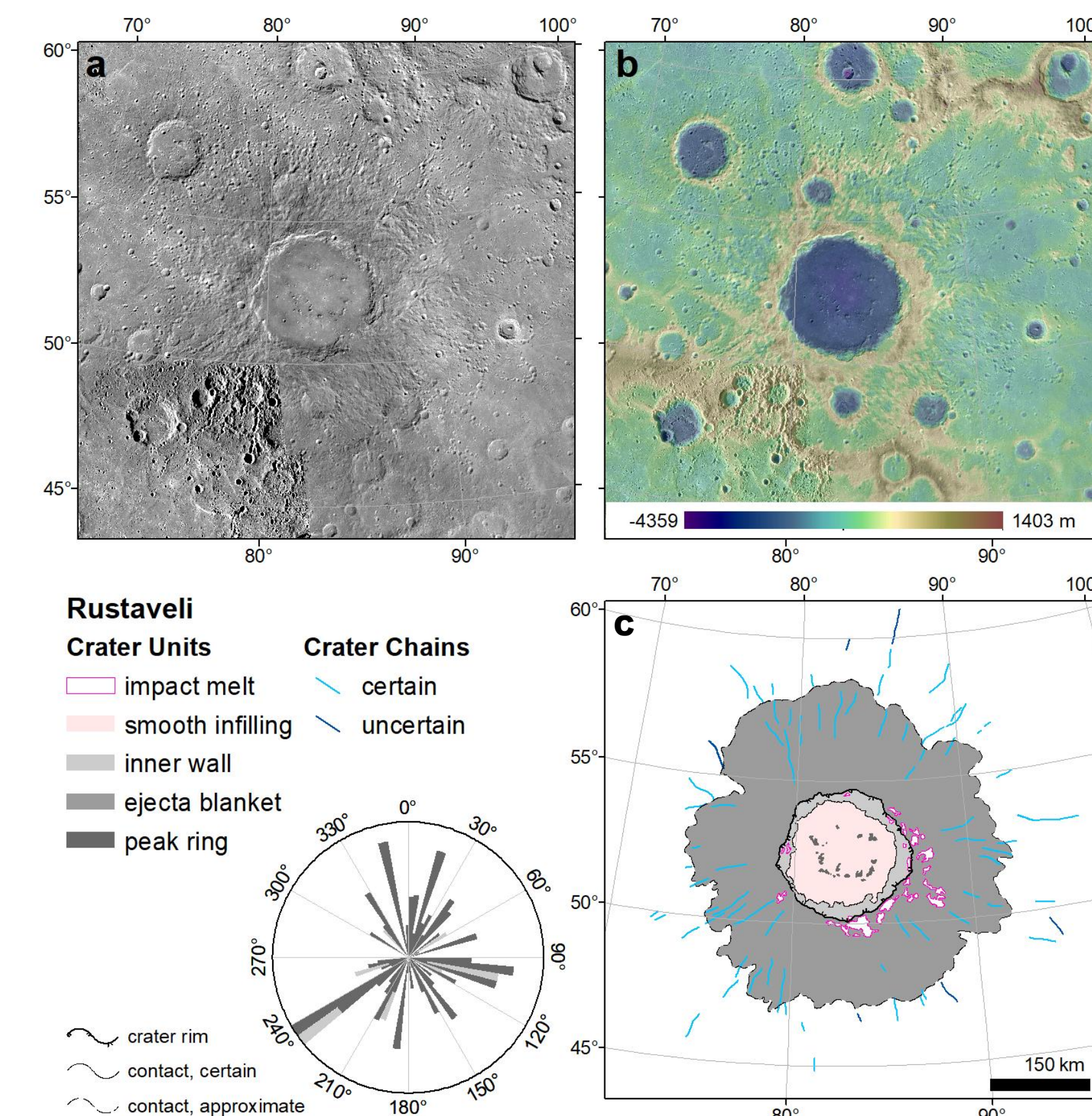
Figure 4 | Rustaveli crater in stereographic projection centered on the crater center (82.74°E; 52.41°N): **a)** BDR (Basemap Data Record) basemap at 166 m/pixel; **b)** DLR stereo-DTM (west of 90°E) and MLA DTM (east of 90°E); **c)** Simplified geological map (from Wright et al., 2019) showing the trend of certain and uncertain secondary crater chains related to the Rustaveli impact. **Bottom-left:** rose diagram analysis of crater chains showing the start and end azimuth of chains indicated by the dark and light bins, respectively.

A | The rim is higher in the southeastern arc than in other parts of the crater [Fig. 4b].

B | Radially textured ejecta extends ~one crater diameter from the rim at all azimuths. However, there is a lack of chains to the WNW [Fig. 4c].

C | The peak-ring appears elliptical, with its long-axis oriented E–W. It seems closer to the south-eastern part of the rim.

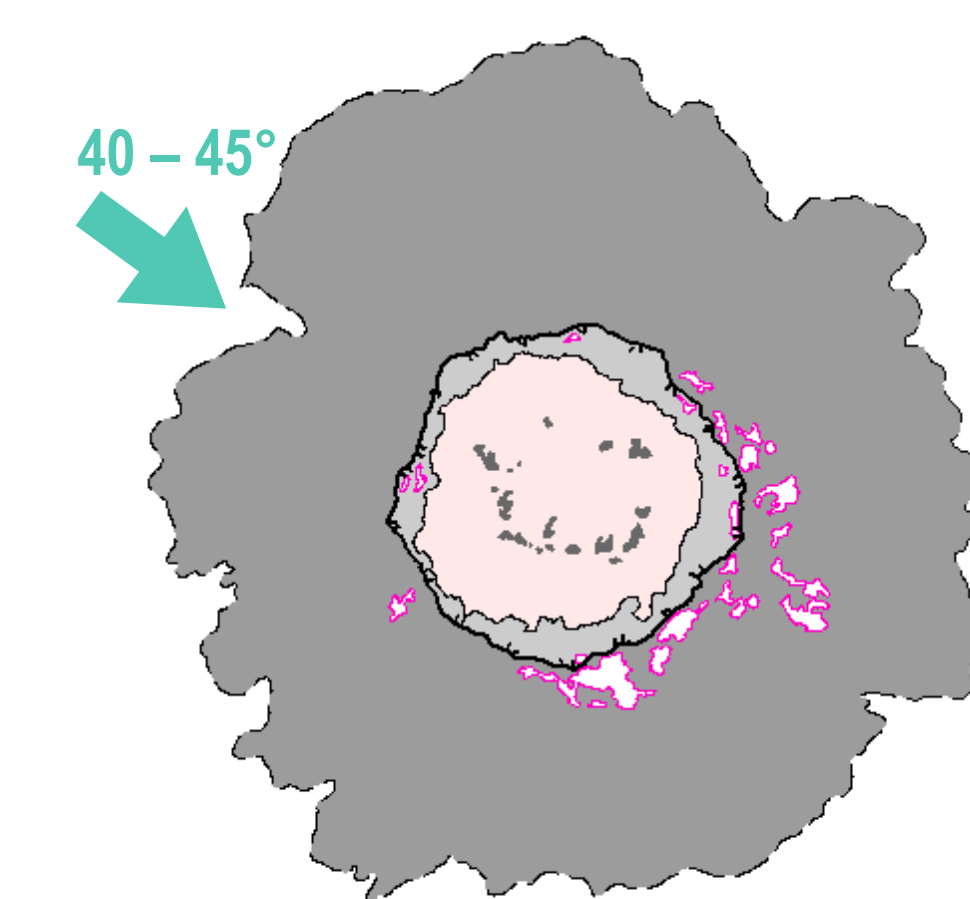**D |** The strongest asymmetry is the concentration of impact melt in ESE, just beyond the crater rim.

QUALITATIVE EVALUATION OF IMPACT DYNAMICS

A | A higher topography of the rim is usually observed in the downrange direction [Gault and Wedekind, 1978].

B | Ejecta radial symmetry is lost for impact angles lower than 35°-45° [Gault and Wedekind, 1978; Pierazzo and Melosh, 2000; Kenkmann et al., 2014]. No forbidden zones are observed for impact angles > 40° [Ekholm and Melosh, 2001].

C | U-shaped central peaks may already occur with impacts < 50° and tend to shift uprange for lower angles, usually showing the opening in the downrange direction [Schultz, 1992; Pierazzo and Melosh, 2000].

D | Impact melt usually focuses downrange for impacts lower than 45° [Gault and Wedekind, 1978; Pierazzo and Melosh, 2000]. For complex craters, melt is more likely driven towards the rim crest lows [Neish et al., 2014].


Figure 3 | Inferred impact direction and angle for Stieglitz. **Case 1)** Based on morphological analysis of cases A, B, C, D; **Case 2)** Based on case D, and location of the deepest chain (red contour).

Figure 5 | Inferred impact direction and angle for Rustaveli based on morphological analysis of cases A, B, C, D.

RELATIONSHIP WITH MAGNETIC ANOMALIES

The method of Parker [Parker, 1991], a unidirectional magnetization direction technique, can locate the magnetized material under certain limits [Oliveira et al., AGU Fall Meeting 2019].

For Stieglitz, an anomaly larger than 3 nT includes most of the ejecta melt locations towards SW. The ejecta melt cluster to the N of the crater corresponds to ~5 nT. The largest strength of ~7 nT closely corresponds to the crater's deepest chain [Fig. 6a].

The dipoles are distributed in the SE-NW direction. The stronger dipoles, probably locating the magnetic carriers, are found mainly at the northwest region outside the crater rim [Fig. 6b].
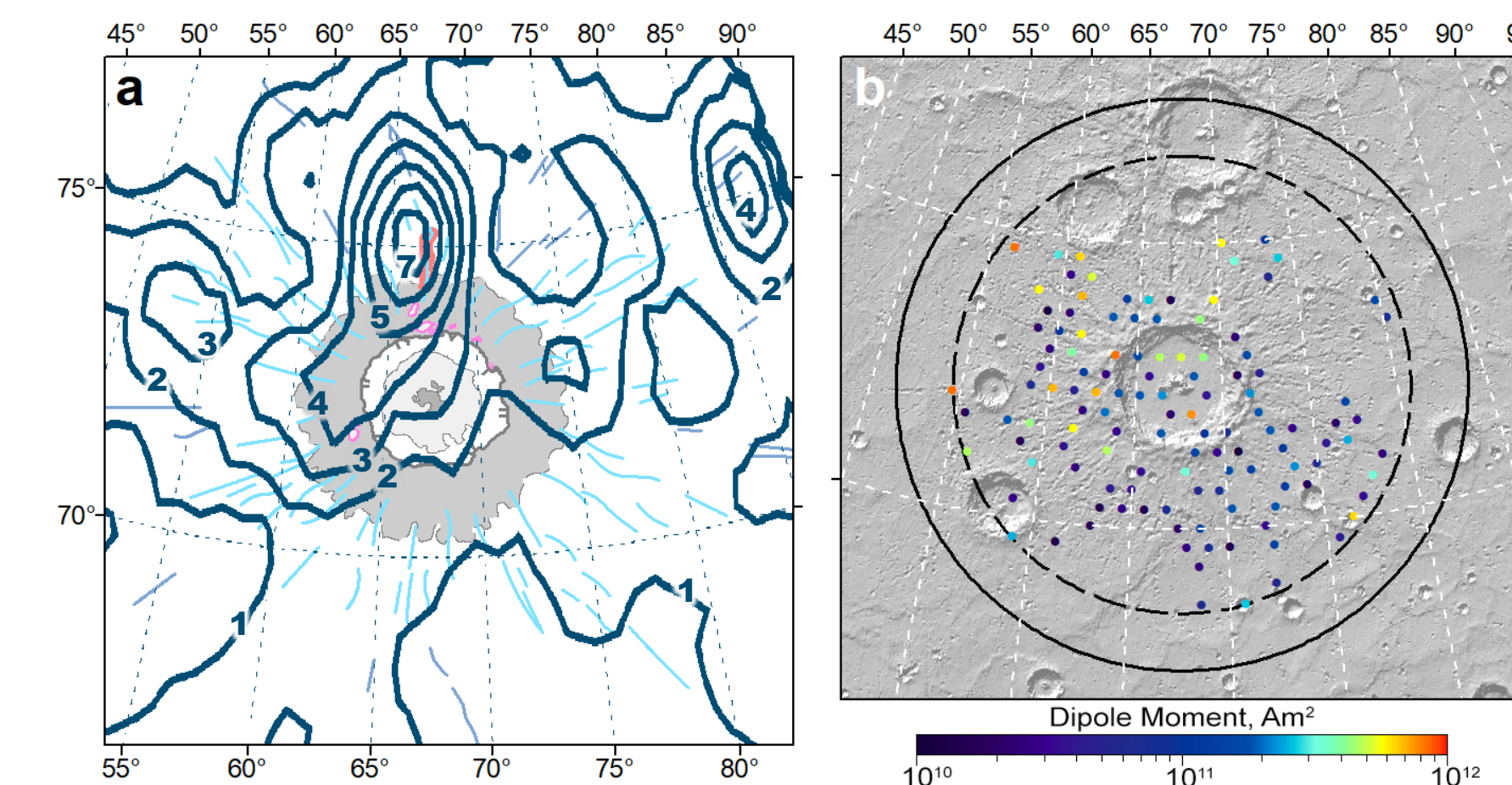
Figure 6 | Results for Stieglitz crater: **a)** Magnetic field intensity with 1 nT contours [Hood et al., 2018] on the geological map; **b)** Dipoles location and intensity on MLA shaded relief.

Rustaveli is associated with a ~5 nT crustal magnetic anomaly centered close the crater's midpoint, although offset ~20 km east-southeast. This offset is somewhat consistent with the downrange direction implied by Rustaveli's impact melt and crater chains distribution [Fig. 7a].

Observing the distribution of the Rustaveli dipoles, we noted that most of the dipoles are located southwest of the studied region. The strongest dipoles are located inside the impact crater rim, also in the southwest of its center [Fig. 7b].
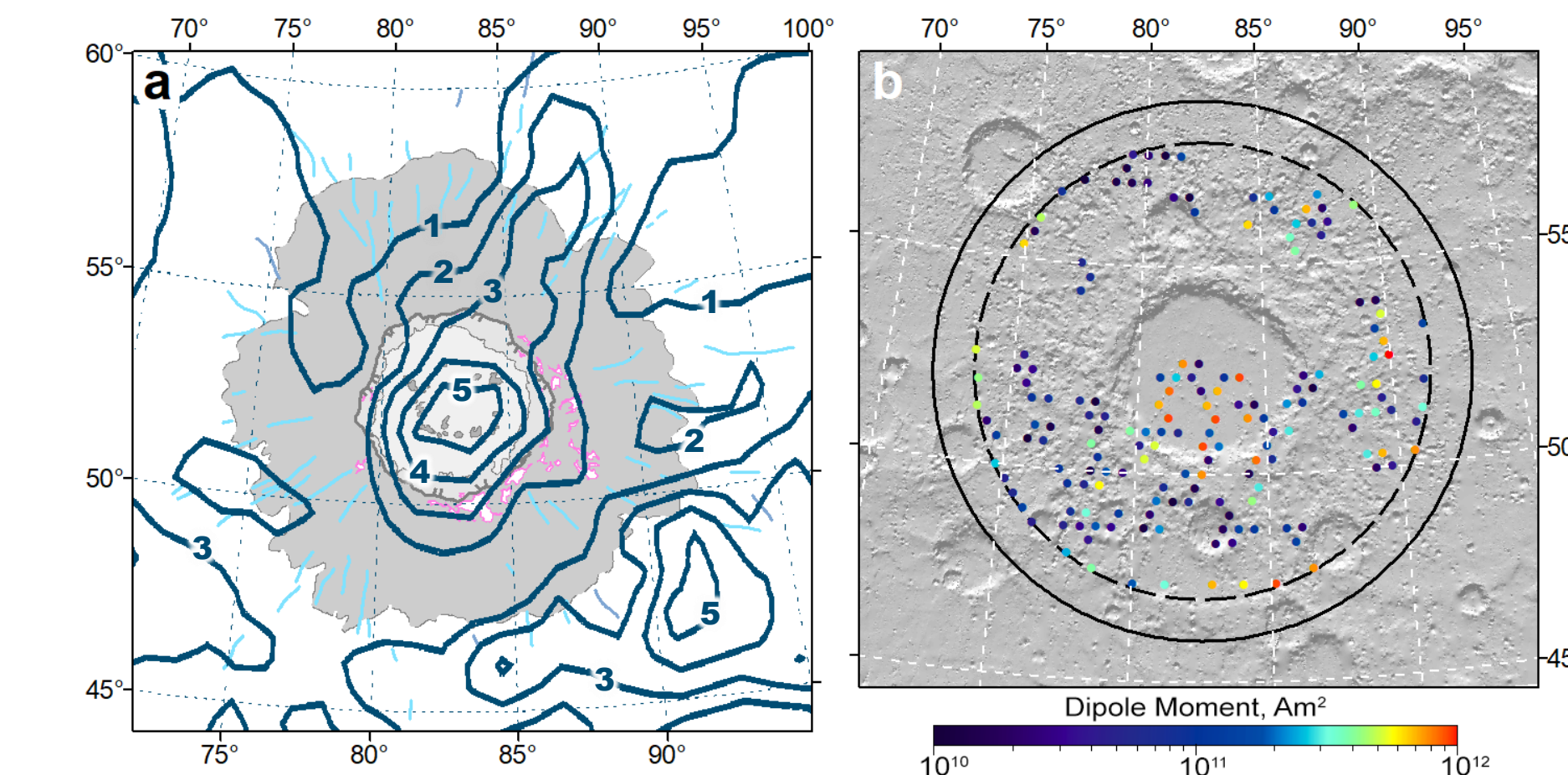
Figure 7 | Results for Rustaveli crater: **a)** Magnetic field intensity with 1 nT contours [Hood et al., 2018] on the geological map [Wright et al., 2019]; **b)** Dipoles location and intensity on MLA shaded relief.

CONCLUSIONS

In both cases, slight asymmetries in the morphology and ejecta distribution show that the magnetic anomalies correlate well with the location of impact melt, and not necessarily the impact direction. Both impact angles were likely 40 – 45°. For the large basin Rustaveli, the melt emplaced in the downrange direction, whereas in the case of the smaller crater Stieglitz, downrange direction remains uncertain; the melt naturally migrated to the topographic lows (Case 1) or in the downrange direction (Case 2).

In both cases, the melt likely recorded the prevailing magnetic field of Mercury after quenching.

References: Ekholmand Melosh, Gephys. Res. Letters28, 2001; Gault and Wedekind, 9thLPSC, 1978; Hood, J. Geophys. Res. Planets121, 2016; Hood et al., J. Geophys. Res. Planets123, 2018; Johnson et al., Science 348, 2015; Kenkmannet al., J. Struct. Geol. 62, 2014; Neishet al., Icarus239, 2014; Parker, J. Gephys. Res. Solid Earth 96, 1991; Pierazzoand Melosh, Annu. Rev. Earth Planet. Sci. 28, 2000; Schultz, LPI Cont. 789, 1992; Wieczoreket al., Science 335, 2012; Wright et al., J. Maps 15, 2019.